Spin waves in an inhomogeneously magnetized stripe

C. Bayer,[1,2] J. P. Park,[1] H. Wang,[1] M. Yan,[1] C. E. Campbell,[1] and P. A. Crowell[1,*]
[1]*School of Physics and Astronomy, University of Minnesota, Minneapolis, Minnesota 55455, USA*
[2]*Fachbereich Physik and Forschungsschwerpunkt MINAS, Technische Universität Kaiserslautern, 67663 Kaiserslautern, Germany*
(Received 19 November 2003; published 1 April 2004)

We have observed collective spin-wave modes in inhomogeneously magnetized $Ni_{0.81}Fe_{0.19}$ thin-film stripes. The stripes, 18 nm thick and 2 μm wide, are studied in an in-plane magnetic field oriented along their short axes. When the magnetic field is on the order of the shape anisotropy field, the equilibrium magnetization near the stripe edges rotates 90 deg over a length scale of order 100 nm–1 μm. Time-resolved Kerr microscopy is used to detect a hierarchy of spin-wave modes in these edge regions. Using a combination of semianalytical theory and micromagnetic simulations, we show that these modes span the entire stripe but can only be detected near the edges, where the effective wave vector is small.

DOI: 10.1103/PhysRevB.69.134401 PACS number(s): 75.30.Ds, 75.40.Gb, 76.50.+g

I. INTRODUCTION

The excitation spectra of ferromagnetic thin-film elements with transverse dimensions on the order of 1 μm or less are influenced profoundly by spatial confinement. At these length scales, the difference in the frequencies of standing spin waves becomes comparable to their linewidth, and the resulting modes can be resolved spectroscopically.[1–3] As the length scale decreases, both exchange and dipolar coupling become important, and the resulting excitations are different in character from the purely magnetostatic modes observed in larger patterned structures.[4,5] An additional class of confined spin waves has been observed in nonellipsoidal systems, in which spin waves with wave vectors parallel to the magnetization can be localized in a region of nonuniform internal magnetic field.[6–8] The internal field in this case is analogous to a confining potential, and it has been shown that the frequencies of the localized spin-wave modes can be determined by a WKB argument in which the spin-wave dispersion relation is a function of position.[6–8] One of the interesting questions raised by the WKB approach is whether it can be applied meaningfully to situations in which the equilibrium magnetization itself is nonuniform. The inhomogeneous magnetization at the edges of a nonellipsoidal particle leads to a modification of the boundary conditions, and the micromagnetic structure may lead to additional edge modes.[9] In some cases, the equilibrium state, although inhomogeneous, may have a relatively simple form, such as the vortex phase of submicron magnetic disks.[10,11] Developing a precise description of the excitation spectra of these nonuniform ground states is an important aspect of the study of magnetic nanostructures.

We have studied the excitation spectra of inhomogeneously magnetized thin-film permalloy stripes using time-resolved Kerr microscopy.[12,13] When the magnetic field, which is applied along the short axis of the stripe, is close to the shape anisotropy field, we find a new class of modes at *higher* frequency than the ordinary precessional mode at the center of the stripe. Although these modes are detected at the edges of the stripe, they are fundamentally different than the localized edge modes observed previously at higher fields.[6–9] The localized modes are confined in regions of inhomogeneous magnetic field at the edges of the stripe, and their eigenfrequencies are *lower* than the frequency of the center mode. In contrast, the new modes, which we call crossover modes, span the entire stripe but are only detectable at the edges, where the magnetization rotates 90 deg to become parallel to the edges. The inhomogeneous magnetization plays an essential role in determining the character of the crossover modes. We show using semianalytical calculations that the wave vector is much smaller at the edges than at the center of the stripe, thus allowing the crossover modes to be observed.

II. RESULTS

Permalloy ($Ni_{0.81}Fe_{0.19}$) stripes, 18 nm thick, 2.3 μm wide, and approximately 1 mm long, are deposited by sputtering through a bilayer resist shadow mask prepared by electron-beam lithography. The substrates are thinned to approximately 25 μm, and the samples are positioned on a coplanar wave guide as shown in Fig. 1.

The applied magnetic field H_a is oriented in the plane and is perpendicular to the long axis of the stripe. We measure the response of the sample to a fast magnetic-field pulse (H_{pulse} in Fig. 1) with a temporal width of 120–150 ps and

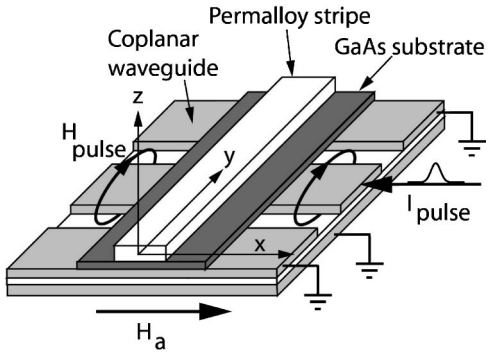

FIG. 1. Schematic drawing of the experimental geometry. The relative dimensions are not to scale. The width of the center conductor of the coplanar waveguide is 30 μm, and the substrate thickness is $\approx$25 μm. The permalloy stripes are 2.3 μm wide, 18 nm thick, and 1 mm long.

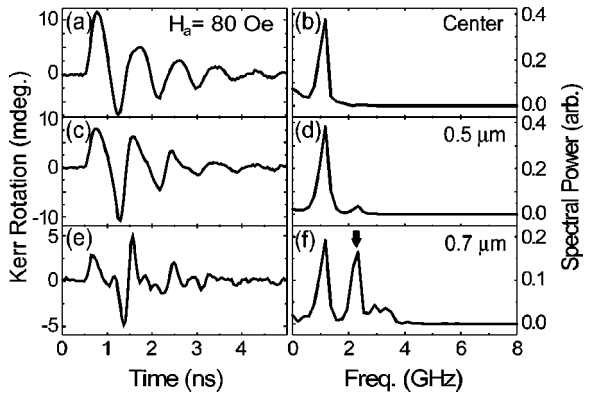

FIG. 2. Time and frequency response (left and right panels) measured at different positions. The positions, relative to the center of the stripe, are indicated in the right-hand panels. The arrow in (f) indicates an edge mode at higher frequency.

an amplitude of ≈ 5 Oe. The direction of the pulsed field is along the stripe. A 150 fs optical probe pulse with a wavelength of 810 nm is focused on the sample using a 100× oil-immersion objective with a numerical aperture of 1.25. The pump-induced change in the polar Kerr rotation of the probe beam is measured as a function of the time delay between the pump and probe pulses. The measured signal is proportional to the z component of the dynamic magnetization. Data obtained in a magnetic field $H_a = 80$ Oe with the objective focused on the center of the stripe are shown in Fig. 2(a).

The response observed in Fig. 2(a) corresponds to nearly uniform precession of the magnetization about the effective field at the center of the stripe. As can be seen in the Fourier transform of the data shown in Fig. 2(b), the spectrum is dominated by a single peak. As the position of the focused probe beam is moved away from the center, the spectrum changes as shown in Figs. 2(d) and 2(f), with an additional peak appearing at higher frequency. A full spectral image of a scan across the stripe can be constructed by measuring the spectrum at each position and converting the spectral intensity to a gray scale. The results for several magnetic fields are shown in Fig. 3, in which the spectral intensity has been normalized by the integrated power measured at each position. This procedure emphasizes the modes near the edges of the stripe, which are much weaker than the center mode in absolute intensity. (The normalization also tends to remove the tails of modes in regions where they overlap with a stronger mode, which enhances the apparent resolution.) The

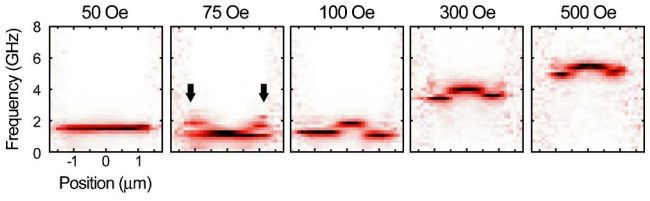

FIG. 3. (Color online) Spectral images of a stripe at several different magnetic fields, normalized as described in the text. The arrows indicate the crossover modes discussed in this paper.

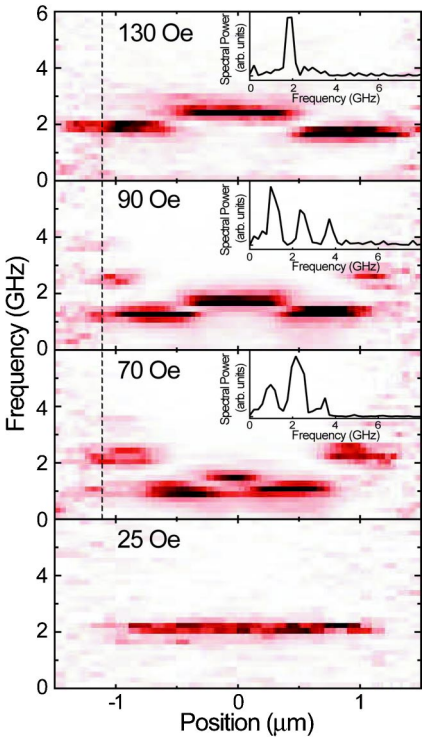

FIG. 4. (Color online) Spectral images of the cross section of a stripe in different applied fields. The insets show the spectra at the position indicated by the dotted line. As discussed in the text, the images extend beyond the physical boundaries of the stripe because of the limited optical resolution.

spectra at low and high fields are well understood. At 50 Oe, the magnetization is nearly parallel to the long axis of the stripe, and the observed response is a single precessional mode. At high fields (>100 Oe), the response consists of a precessional mode spanning most of the stripe and a lower-frequency mode localized at each edge.[6–8] This paper focuses on the field range of 60–130 Oe, in which modes are observed near the edges of the stripe at higher frequencies than the center mode. These excitations are indicated by arrows in Figs. 2(f) and 3.

Figure 4 shows frequency domain images of a 2.3 μm wide stripe for fields from 25 Oe to 130 Oe. (Note that the images correspond to the convolution of the z component of the dynamic magnetization with the optical resolution function. As a result, the mode profiles extend beyond the physical boundary of the stripe.) The edge modes observed at 130 Oe are the localized modes seen in Fig. 3 at higher fields. At 70 and 90 Oe, a separate set of modes is observed at frequencies above the center mode. At lower fields a single mode emerges, although the total intensity becomes extremely weak as the field approaches zero. The insets of the top three panels of Fig. 4 show spectra obtained with the probe beam positioned 1.2 μm from the center of the stripe, corresponding to the position indicated by the dotted line. At 130 Oe, only the ordinary localized mode is observed at this position. The additional peaks at 90 and 70 Oe are the higher-frequency crossover modes.

All of the mode frequencies observed at different positions on the stripe are shown in Fig. 5(a) as a function of

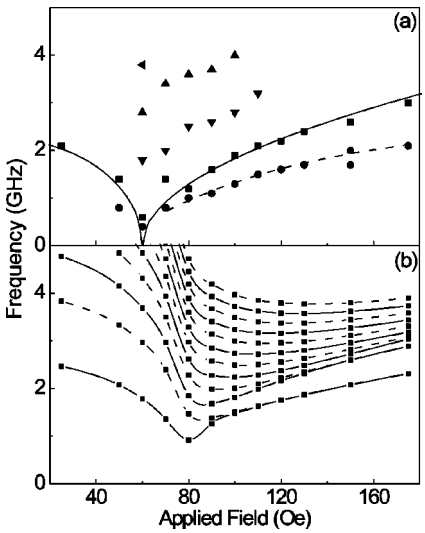

FIG. 5. (a) The measured frequencies as a function of the applied field. The solid curve is the frequency of the ordinary FMR mode calculated as described in the text. The points along the dashed curve are the localized modes. (b) The points in the lower panel indicate the normal mode frequencies calculated as described in the text.

magnetic field. The frequencies shown are those of peaks with an amplitude at least five times the background noise level. The solid curve is the frequency of the ordinary ferromagnetic resonance (FMR) mode of the stripe, which is calculated under the assumption that the magnetization is uniform and that it undergoes coherent rotation. The shape anisotropy energy was determined by approximating the stripe as an ellipsoid with demagnetizing factors $N_x = H_d/M_s$, $N_y = 0$, and $N_z = 4\pi - H_d/M_s$, where the demagnetizing field $H_d = 60$ Oe was taken from the location of the experimental minimum in the FMR frequency. The points along the dashed curve at high fields are the localized modes discussed above. The points at higher frequencies from 60–120 Oe are due to the crossover modes that appear near the edges of the stripe.

III. DISCUSSION

The overall structure of the spectral images shown in Fig. 4 is the same for different stripes of the same width: in the field regime around 90 Oe, a set of modes appears at the edges of the stripe. The details of the spectrum, such as the exact frequencies of the modes, vary from stripe to stripe, and there is a significant asymmetry in the images between the left and right sides of a single stripe. We focus here on a global description of the spin-wave spectrum, although there are some features that may depend on the micromagnetic structure of a particular stripe.

The key observation about the field regime in which the additional edge modes are observed in Fig. 4 is that the magnetization is nonuniform over a significant fraction of the width of the stripe. The local magnetization direction is determined by a competition between the shape anisotropy field, which favors a magnetization parallel to the edges of the stripe, and the applied field, which is along its width. Figure 6(a) shows the two in-plane components of the magnetization of a 2.3 μm stripe calculated micromagnetically for an applied field of 90 Oe along $\hat{x}$. The magnetization at the center of the stripe is parallel to the applied field while it is nearly parallel to the stripe at the edges. Between these two extremes the magnetization rotates smoothly over a length scale of 0.5 μm. Figure 6(b) shows the corresponding effective field H_{eff}, including the applied, demagnetizing, and exchange fields. H_{eff} differs significantly from zero only in the region where the magnetization is parallel to the applied field.

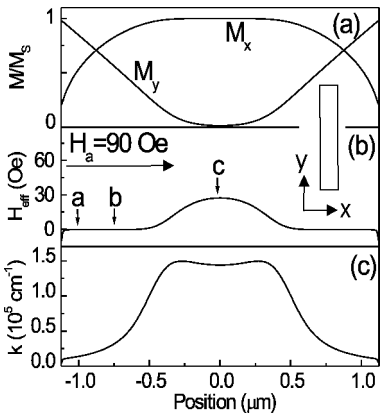

FIG. 6. (a) The two in-plane components of the static equilibrium magnetization are shown as a function of x in an applied field of 90 Oe along $\hat{x}$. (b) The corresponding effective field H_{eff}. The positions a, b, and c are 1.0, 0.75, and 0 μm from the center of the stripe. (c) The wave vector k, evaluated from the dispersion relation as described below, is shown for one of the crossover modes as a function of x. The inset shows the coordinate system.

The important question in the interpretation of the experimental results is the relationship between the magnetization profile shown in Fig. 6(a) and the observed spin-wave spectrum. We will now show that the higher-frequency modes seen in Fig. 4 extend over the entire stripe although they can be observed only at the edges. This is in contrast to the localized edge modes, for which the wave vector k becomes imaginary in the center of the stripe. As will be shown below, it is possible to calculate the wave vector k of a particular mode as a function of position once the magnetization profile is known. The result for one of the crossover modes in a field of 90 Oe is shown in Fig. 6(c). The regions of small wave vector near the edges of the stripe allow for these modes to be detected.

We begin our analysis by considering a one-dimensional wave equation derived from the Landau-Lifshitz-Gilbert (LLG) equation[14]

$$(1+\alpha^2)\frac{\partial \mathbf{M}}{\partial t} = -|\gamma|\mathbf{M}\times\mathbf{H}_{eff} - \frac{|\gamma|\alpha}{M_S}\mathbf{M}\times(\mathbf{M}\times\mathbf{H}_{eff}), \tag{1}$$

in the limit of small deviations of $\mathbf{M}(x,t)$ from the static magnetization $\mathbf{M}_0(x)$. The effective field is given by

$$\mathbf{H}_{eff}(x,t) = \mathbf{H}_a + \frac{2A}{M_S^2}\nabla^2\mathbf{M}(x,t) + \int_{-w/2}^{w/2} \tilde{\mathbf{G}}(x,x') \cdot \mathbf{M}(x',t)dx', \qquad (2)$$

where $\mathbf{H}_a$ is the applied field, $w = 2.3$ μm is the width of the stripe, $A = 1.3 \times 10^{-6}$ erg/cm is the exchange constant, and $M_s = 770$ emu/cm^3 is the saturation magnetization. All calculations were carried out with a gyromagnetic ratio $\gamma/2\pi = 2.95$ GHz/kOe and $\alpha = 0.008$. The static part $\mathbf{M}_0(x)$ of $\mathbf{M}(x,t) = \mathbf{M}_0(x) + \mathbf{m}(x,t)$ is determined from full micromagnetic simulations, and the dynamic part $\mathbf{m}(x,t) = \mathbf{m}(x)e^{i\omega t}$, which is perpendicular to $\mathbf{M}_0(x)$, is a solution of the linearized LLG equation. The Green's function of the dipole-dipole interaction $\tilde{\mathbf{G}}(x,x')$ can be found in Ref. 15. Equation (1) can then be reduced to an eigenvalue problem, which is solved numerically.[16]

Figure 5(b) shows the eigenfrequencies calculated for the lowest several modes as a function of the applied field. Similar calculations over a wider field range have recently been reported and are in qualitative agreement with the results shown here.[17] For fields below 40 Oe the mode profiles and frequencies match previous results[15,18] for a stripe magnetized along its length, and the results above 120 Oe correspond to the case of a stripe magnetized along its short axis. The lowest pair of degenerate modes above 90 Oe are the localized modes observed previously.[6–8] We focus here on the region near 80 Oe in Fig. 5(b). Although the field corresponding to the minimum frequency of the lowest modes is significantly higher in the calculations than in experiment, the evolution of the lower branches in Fig. 5(b) agrees qualitatively with that seen in the experimental data of Fig 5(a). In contrast, excitations in the higher branches are observed in experiment only in the crossover regime above 60 Oe.

Although there are not enough data to assess the quantitative agreement between the frequencies of the higher modes in Figs. 5(a) and 5(b), profiles of the z component of the dynamic magnetization provide a clear indication of why the crossover modes are observed only near the edges of the stripe. The lowest 12 mode profiles are shown in Fig. 7 for a field of 90 Oe. The modes are shown in pairs and are indexed by the number of nodes. As the mode index increases, additional nodes appear in the center of the stripe, in the region where the magnetization is parallel to the short axis. For all modes with $n > 2$, the distance between the edge of the stripe and the first *internal* node is at least a factor of 2 greater than the distance between the internal nodes. This edge region is the only area where the m_z does not average to zero over the diameter of the optical spot ($\approx$800 nm) used in the experiment. As the mode index increases, the distance to the first internal node decreases, which is why the spectral weight observed in the experiment (see Fig. 4) moves further towards the edges of the stripe as the frequency increases.

A second question concerns how the crossover modes are driven, since they clearly have characteristic wavelengths smaller than the width of the stripe while H_{pulse} is essentially uniform over the entire stripe. The nonuniform magnetization again plays an important role, since the resulting dynamic torque $\mathbf{M}(x,t) \times \mathbf{H}_{pulse}(t)$ has significant spatial Fourier components at the wave vectors of the higher modes. In contrast, it is extremely difficult to drive higher-order modes in the low-field regime, in which the magnetization is aligned along the stripe. In this case the pulsed field is parallel to the magnetization, and the torque is therefore extremely weak. Furthermore, the torque is uniformly distributed across the stripe, and so the coupling to higher-order modes occurs only by the rapidly decreasing Fourier components of the square-wave envelope. This is why no higher modes are observed in Fig. 5(a) for fields below 60 Oe. At the highest fields, there is some torque generated at the extreme edges of the stripe, providing coupling to the localized modes, but there is essentially no spatial overlap of the torque with the higher-order modes. A test of this argument can be made using dynamic micromagnetic simulations with a realistic pulse profile. Simulations of the full Landau-Lifshitz-Gilbert equation were conducted using the object-oriented micromagnetic framework (OOMMF).[19] The stripe was discretized along the x and z axes (see Fig. 1) with a cell size of 4.5 nm. The translational symmetry along y was accounted for using OOMMF's infinite tube convention. To obtain the initial condition for each magnetic field, the system was relaxed from a state of homogeneous magnetization $M_0\hat{y}$ with a large Gilbert damping parameter $\alpha = 0.5$. The relaxed state was then taken as the initial condition for the dynamical calculation, which was undertaken with a damping parameter of $\alpha = 0.008$. A Gaussian pulse with a full width at half maximum (FWHM) of 150 ps and an amplitude of 10 Oe was applied, and the response over the next 10 ns was calculated using 10 ps time steps during the pulse and 20 ps steps after the pulse.

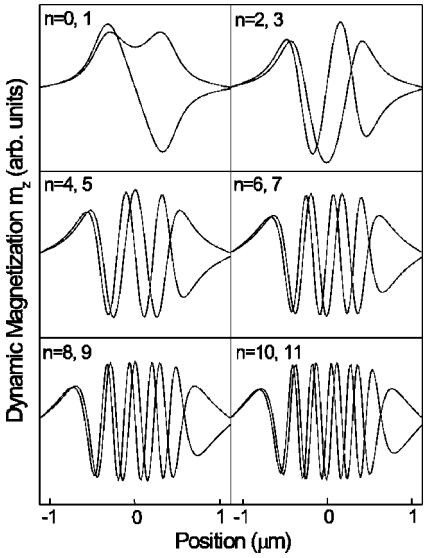

FIG. 7. The amplitude m_z of the lowest 12 eigenmodes of the linearized form of Eq. (1) in an applied field of 90 Oe. The labels indicate the number of nodes.

The results of the simulations are compared with the experiment at fields of 90 and 125 Oe in Fig. 8. Panels (a) and (c) show experimental spectral images. Panels (b) and (d)

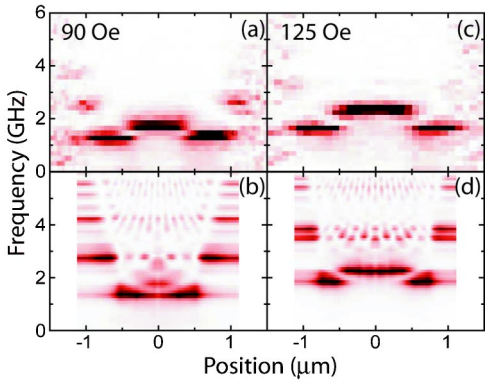

FIG. 8. (Color online) The upper panels (a) and (c) show experimental spectral images of the cross section of the stripe at fields of 90 and 125 Oe. The lower panels (b) and (d) show simulated images obtained as described in the text. The spectra are normalized by the integrated power at each position.

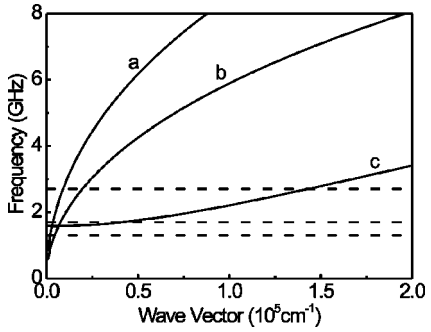

FIG. 9. The dispersion relation calculated at three points along a cross section of the stripe of width 2.3 μm in an applied field of 90 Oe. The letters *a*, *b*, and *c* indicate positions 1.0, 0.75, and 0 μm from the center of the stripe. These positions are also indicated in Fig. 6. The three dashed lines indicate the frequencies of the lowest modes found in simulations.

show spectral images obtained from the time-domain simulations, which were processed in the same manner as the experimental data. All images are normalized by the total spectral weight at each position. These results show clearly that the uniform pulsed field can drive the crossover modes by coupling to the nonuniform magnetization. The mode structure near the edges of the stripe is qualitatively similar in both cases, with the weight moving closer to the edges with higher mode index as noted above. The structure in the center of the stripe in simulations cannot be observed in experiment due to the spatial averaging over the diameter of the optical spot.

Although the simulations show some of the important qualitative features of the experiment, there are several discrepancies, the most important of which is the apparent shift in field scale. The localized modes (at frequencies below the center mode) in experiment are already evident at 90 Oe but do not appear clearly until 125 Oe in the simulations. Although the detailed micromagnetic structure of the stripe will be sensitive to imperfections in the edges, we do not have a quantitative explanation for the shift. The coupling to particular modes depends strongly on the spatial distribution of the dynamic torque generated by the field pulse, but we do not have a simple physical picture predicting which modes will be driven most effectively.

A final way of looking at the region of inhomogeneous magnetization is by considering the dispersion relation at each position in the stripe. This is the same philosophy applied in the WKB argument used previously to described localized spin waves,[6,7] except that in the current case both the internal field and the dipole-dipole matrix element vary with position. The dynamic torque in our experiment couples only to wave vectors along the short axis of the stripe. For a given orientation of **M**, the dispersion relation for spin-waves propagating along the short axis was calculated using the magnetization and internal field profiles from Figs. 6(a) and 6(b) and the dipole-exchange dispersion relation of Kalinikos and Slavin.[20] The effective field $H_{eff}(x)$ and angle $\theta(x)$ between **M** and $\hat{x}$ determine the dispersion relation at each position x across the stripe. The dispersion relations for three values of x in a field of 90 Oe are shown in Fig. 9. These positions are also indicated by the letters *a*, *b*, and *c* in Fig. 6.

At the edge of the stripe, the magnetization is nearly perpendicular to the wave vector **k** and the corresponding dispersion relation, indicated (*a*) in Fig. 9, is that of the usual Damon-Eshbach modes.[21] In the center of the stripe, $\mathbf{M}||\mathbf{k}$, and the dispersion relation (*c*) is that of the backward volume magnetostatic (BWVMS) modes.[20] The frequencies of the three lowest modes found in simulations are shown as the dashed lines in Fig. 9. For the third and higher modes, the wave vector at which the frequency intersects the BWVMS dispersion relation agrees with the value determined from the spacing between the nodes in Fig. 7. Near the edge of the stripe there is a minimum wave vector determined by the intersection of the dashed curve with the Damon-Eshbach dispersion relation (*a*). The wave vector for the third mode (the upper dashed line in Fig. 9) is shown as a function of position in Fig. 6(c), and it is clear that the wave vector at the center of the stripe is about 10 times larger than at the edge. The crossover modes are thus characterized by two different spatial regimes: a dipolar region near the edge of the stripe and an exchange-dominated region of large wave vector near the center of the stripe. In contrast to the two higher modes, the lowest-frequency mode does not intersect the dispersion relation (*c*) at the center of the stripe. This is a signature of the incipient spin-wave localization and becomes more pronounced as the BWVMS dispersion relation at the center of the stripe shifts upward with increasing applied field. Unlike the crossover modes, the localized modes do not propagate in the center of the stripe. This is the important distinction between the two types of modes, even though they are both observed at the edges.

As in the spin-wave localization problem, it is not obvious *a priori* that the usual adiabatic condition for WKB theory is satisfied.[22] In the edge regions, the dispersion relation changes on a length scale comparable to the wavelength and the boundary conditions are not known exactly. Nonetheless, for a given frequency it is straight forward to calculate the

wave vector of each mode as a function of position using the magnetization profile shown in Fig. 6. The Bohr-Sommerfeld integral

$$\phi(n) = \int_{-w/2}^{w/2} k_n(x)\,dx, \tag{3}$$

can then be calculated, where w is the width of the stripe and n is the number of nodes. We have calculated ϕ for the modes at 90 Oe with 2–16 nodes, finding $\phi(n) = \phi_0 + n\pi$, with $\phi_0 = (0.83 \pm 0.02)\pi$. The phase difference $\phi(n) - \phi(n-1)$ differs from π by at most 5%. The relative success of the WKB approach for the crossover modes suggests that it is meaningful to think of a local dispersion relation, even in cases of a strongly inhomogeneous magnetization.

As a final note, it is important to recognize that the inhomogeneous structure considered here shares some of the features of a 90 deg domain wall. In this case, it is reasonable to ask whether the frequencies of the crossover modes are determined by the dipolar coupling between the edges of the stripe and a domain corresponding to the center region. If this were true, it would be more appropriate to describe the crossover modes as domain-wall resonances rather than spin waves.[23] The models above, which demonstrate the exchange character of the modes near the center of the stripe, are clearly consistent with the spin-wave picture. Although the exchange-dominated region cannot be observed using our optical probe, we have not found an alternative model that explains the observed evolution of the modes in the edge regions. There are some features of our data, such as the asymmetry between the left and right edges of the stripe and variations in the crossover mode frequencies from stripe to stripe that are likely to depend on micromagnetic structure not included in the simple description presented here. Nonetheless, the experiment clearly demonstrates that the inhomogeneous system has well-defined collective modes, including higher-frequency excitations that are accounted for in the spin-wave model.

ACKNOWLEDGMENTS

This work was supported by NSF Grant No. DMR 99-83777, the University of Minnesota MRSEC (Grant No. DMR 02-12032), Grant No. ONR N/N00014-02-1-0815, the Minnesota Supercomputing Institute, and the Studienstiftung des deutschen Volkes (C.B.). We thank C. Leighton for assistance with sample preparation and S. O. Demokritov for useful discussions.

*Electronic address: crowell@physics.umn.edu

[1] J. Jorzick, S.O. Demokritov, C. Mathieu, B. Hillebrands, B. Bartenlian, C. Chappert, F. Rousseaux, and A.N. Slavin, Phys. Rev. B **60**, 15 194 (1999).

[2] Y. Roussigné, S.M. Chérif, C. Dugautier, and P. Moch, Phys. Rev. B **63**, 134429 (2001).

[3] Z.K. Wang, M.H. Kuok, S.C. Ng, D.J. Lockwood, M.G. Cottam, K. Nielsch, R.B. Wehrspohn, and U. Gösele, Phys. Rev. Lett. **89**, 027201 (2002).

[4] S. Tamaru, J.A. Bain, R.J.M. van de Veerdonk, T.M. Crawford, M. Covington, and M.H. Kryder, J. Appl. Phys. **91**, 8034 (2002).

[5] W.K. Hiebert, G.E. Ballentine, and M.R. Freeman, Phys. Rev. B **65**, 140404 (2002).

[6] J. Jorzick, S.O. Demokritov, B. Hillebrands, M. Bailleul, C. Fermon, K. Guslienko, A.N. Slavin, D. Berkov, and N.L. Gorn, Phys. Rev. Lett. **88**, 047204 (2002).

[7] J.P. Park, P. Eames, D.M. Engebretson, J. Berezovsky, and P.A. Crowell, Phys. Rev. Lett. **89**, 277201 (2002).

[8] C. Bayer, S.O. Demokritov, B. Hillebrands, and A.N. Slavin, Appl. Phys. Lett. **82**, 607 (2003).

[9] M. Bailleul, D. Olligs, and C. Fermon, Phys. Rev. Lett. **91**, 137204 (2003).

[10] R.P. Cowburn, D.K. Koltsov, A.O. Adeyeye, M.E. Welland, and D.M. Tricker, Phys. Rev. Lett. **83**, 1042 (1999); T. Shinjo, T. Okuno, R. Hassdorf, K. Shigeto, and T. Ono, Science **289**, 930 (2000).

[11] J.P. Park, P. Eames, D.M. Engebretson, J. Berezovsky, and P.A. Crowell, Phys. Rev. B **67**, 020403 (2003).

[12] W.K. Hiebert, A. Stankiewicz, and M.R. Freeman, Phys. Rev. Lett. **79**, 1134 (1997).

[13] Y. Acremann, C.H. Back, M. Buess, O. Portmann, A. Vaterlaus, D. Pescia, and H. Melchior, Science **290**, 492 (2000).

[14] J. Miltat, G. Albuquerque, and A. Thiaville, in *Spin Dynamics in Confined Magnetic Structures I*, edited by B. Hillebrands and K. Ounadjela (Springer-Verlag, Berlin, 2002).

[15] K.Yu. Guslienko, S.O. Demokritov, B. Hillebrands, and A.N. Slavin, Phys. Rev. B **66**, 132402 (2002).

[16] C. Bayer, Diplomarbeit in Physik, Technische Universität Kaiserslautern, Germany, 2003.

[17] Y. Roussigné, S.M. Chérif, and P. Moch, J. Magn. Magn. Mater. **268**, 89 (2004).

[18] Y. Roussigné, S.M. Chérif, and P. Moch, J. Magn. Magn. Mater. **263**, 289 (2003).

[19] M.J. Donahue and D.G. Porter, NIST Interagency Report No. NISTIR 6376 (unpublished).

[20] B.A. Kalinikos and A.N. Slavin, J. Phys. C **19**, 7013 (1986). We use their Eq. (45) with the dipole matrix element P_{nn} calculated from Eq. (A12).

[21] R.W. Damon and J.R. Eshbach, J. Phys. Chem. Solids **19**, 308 (1961).

[22] L.D. Landau and E.M. Lifshitz, *Quantum Mechanics: Non-Relativistic Theory*, 3rd ed. (Pergamon, Oxford, 1977).

[23] U. Ebels, L.D. Buda, K. Ounadjela, and P.E. Wigen, in *Spin Dynamics in Confined Magnetic Structures I*, edited by B. Hillebrands and K. Ounadjela (Springer-Verlag, Berlin, 2002).